

MECHANISM OF LIGHT-PARTICLE EMISSION

Shoji Nagamiya†

Nuclear Science Division, Lawrence Berkeley Laboratory,
University of California, Berkeley, California 94720, U. S. A.

DISCLAIMER

This document is prepared for the U.S. Department of Energy under contract number W-7405-ENG-48. It contains information that is proprietary to the U.S. Government and is not to be distributed outside the government without the express written permission of the U.S. Government. This document is prepared for the U.S. Department of Energy under contract number W-7405-ENG-48. It contains information that is proprietary to the U.S. Government and is not to be distributed outside the government without the express written permission of the U.S. Government.

The work was supported by the Director, Office of Energy Research, Division of Nuclear Physics of the Office of High Energy and Nuclear Physics of the U.S. Department of Energy under Contract W-7405-ENG-48. It was also supported by the INS-LBL Collaboration Program.

MECHANISM OF LIGHT PARTICLE EMISSION

Shoji Nagamiya†

Nuclear Science Division, Lawrence Berkeley Laboratory,
University of California, Berkeley, California 94720, U. S. A.

1. INTRODUCTION

Since I was asked to deliver two talks, one today and the other on Thursday, I would like to split my subject in the following way: Today, I will discuss a general overview of the field of high-energy nuclear collisions studied from light particle spectra, pions, kaons, lambdas, protons, deuterons, and light composite fragments. Specifically, I will discuss the basic reaction mechanism that determines the main features of particle emission such as the energy and angular distributions, the multiplicity, the production rate, the projectile and target mass dependences, the beam-energy dependences, etc. On Thursday, I will describe more specific topics that are not yet understood in terms of the current theoretical framework. Also, future possibilities in high-energy heavy-ion research will be discussed then.

The organization of today's talk is as follows. Since some of the audience may not be familiar with the field, I will first describe very general features of high-energy nuclear collisions (Sec. 2). The major question here is what characterizes these collisions. Second, I will discuss proton emission (Sec. 3), since the proton is the dominant particle emitted at a large angle. Thirdly, the mechanism of composite-fragment formation is discussed (Sec. 4). The fourth topic is pion production (Sec. 5), in which I will extract some important data out of widely collected pion data. In the fifth, I will discuss the strange particle production (Sec. 6), and finally I will give a summary in Sec. 7.

2. WHAT CHARACTERIZES HIGH-ENERGY NUCLEAR COLLISIONS?

As an introduction the de Broglie wave length of incident nucleons inside the projectile nucleus (in the nucleon-nucleon (NN) c.m. frame) is plotted in Fig. 1 as a function of the beam energy per nucleon (in the laboratory frame). At about 1 GeV per nucleon the de Broglie wave length is about 0.3 fm which is much shorter than the typical internucleon distance ($d \approx 1.8$ fm). This fact implies that incident nucleons inside the projectile can recognize the individuality of target nucleons. Therefore, it is likely that individual NN collisions determine the basic dynamics of nucleus-nucleus collisions at high energies. Nuclear collisions at beam energies above a few 100 MeV per nucleon are thus very different from very low energy nuclear collisions ($E_{\text{beam}}/A < 50$ MeV) for which the de Broglie wave length is comparable to the whole nuclear radius. There the mean field approximation is more or less justified.

At beam energies above 10 GeV per nucleon the de Broglie wavelength is less than $1/10$ of the nucleon size. Therefore, at these energies the internal structure of the nucleon might show up, and perhaps the role of quark-quark or quark-gluon interactions becomes more important there. However, in the beam energy region of $E_{\text{beam}}/A \approx 1$ GeV, which is the main focus of the present School, the nucleus-nucleus collision is, to a first order approximation, regarded as an ensemble of NN collisions.

Then, what is the difference between the NN collision and the nucleus-nucleus collision at high energies? One obvious feature of the nucleus beam is, as seen in Fig. 2 (upper), that nucleons are packed closely within a small radius of a few fm. Consequently, the local nucleon flux density is about 10^{19} nucleons/cm²/sec, which of

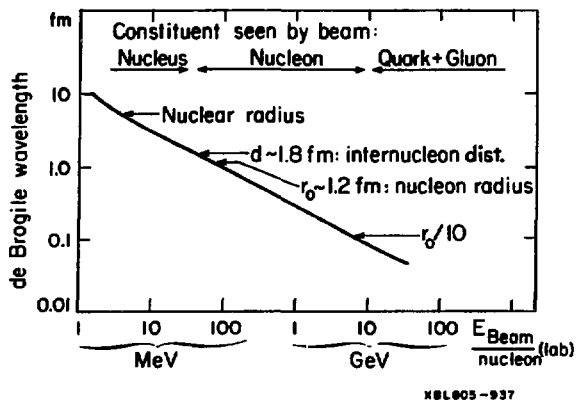


Fig. 1

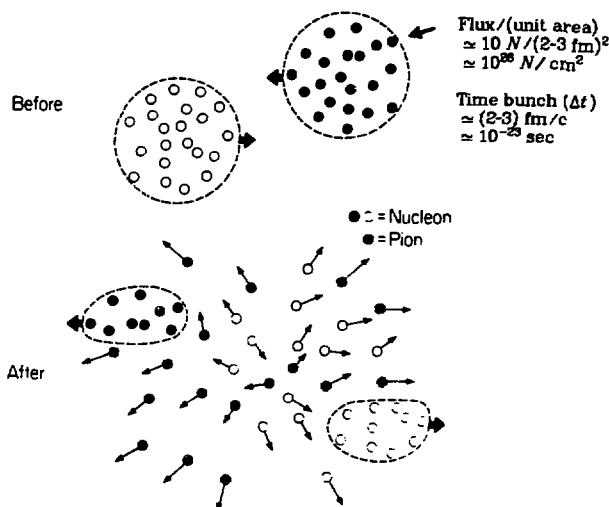


Fig. 2

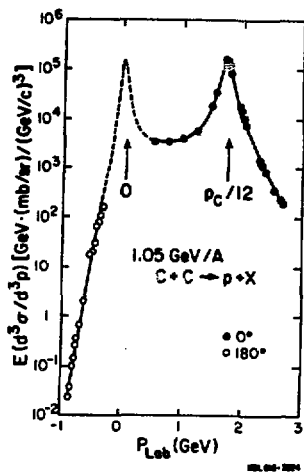


Fig. 3

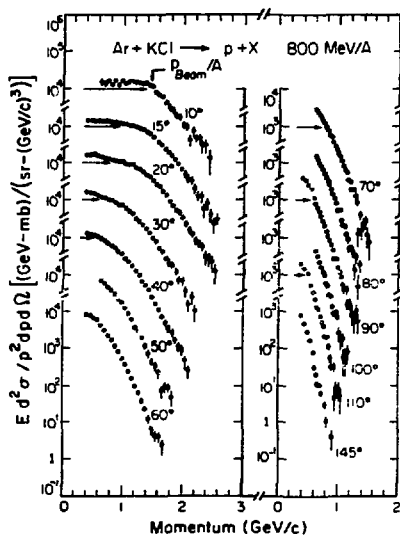


Fig. 4

course cannot be obtained by any proton accelerator. This "packing" feature of nucleons introduces, in fact, a great advantage of using nucleus beams instead of nucleon beams.

If NN collisions determine the basic dynamics, then what do we expect after the collision? As shown in Fig. 2 (lower), some nucleon groups which are located in the non-overlapped regions between the projectile and target will just pass through, keeping their initial velocities. These nucleon groups are called spectator. On the other hand, in the overlap region, nucleons interact violently with each other and scattered over a wide range of angles and momenta. These nucleons are called participant, and such a picture is called the participant-spectator model.¹

Let us look at the data. Shown in Fig. 3 are the proton momentum spectra measured at 0° (Ref. 2) and 180° (Ref. 3) in 1.05 GeV per nucleon C + C collisions. Two peaks are clearly observed, one at $p_p = p_C/12$, namely at the beam velocity, and the other at $p_p = 0$ (at the target velocity). They are most likely from spectator nucleons.

How about the data at large angles? Shown in Fig. 4 are the proton spectra in 800 MeV per nucleon Ar + KCl collisions measured at angles from 10° to 145° (Ref. 4). The spectra are very smooth as a function of the proton momentum and extend up to fairly high momenta. If these cross sections are integrated over angles and momenta, then the total cross section is about 15 barns which is very close to the expected total cross section^{4,5} (18 barns) of participant protons from the simple participant-spectator model.

Two macroscopic quantities, the mean free path (λ) and the collision radius (R), play an important role in collision dynamics. At $E_{\text{beam}}/A \approx 1$ GeV, these two values have recently been determined to be $\lambda \approx 2.4$ fm [Ref. 6] and $R \approx 2.4$ fm [Refs. 7-10,4]. If $\lambda \gg R$, then the nucleus is almost transparent and each nucleon experiences at most one NN collision, and consequently the nuclear collision is described as a simple superposition of single NN collisions without any rescattering. This is called the *direct* limit. The hard-collision model¹¹ is applicable in this limit. On the other hand, if $\lambda \ll R$, then each nucleon experiences successive multiple collisions, and the available kinetic energy tends to be shared among all participating nucleons. This is called the *thermal* limit. Most of the macroscopic models, such as the thermal¹² or the hydrodynamical¹³ models, are based on this assumption. The actual situation is, however, between these two limits, since $\lambda \approx R$. This is one of the complexities of the reaction mechanism of high energy nuclear collisions.

Now, we have the following general observations. Individual NN collisions seem to determine the basic dynamics of the nucleus-nucleus collision. Geometrically, the high energy nucleus beam is characterized by a high local nucleon flux density. Kinematically, data at large angles tend to reflect more features of the participant region, whereas the data at around the projectile and target velocities reflect more features of the spectator region. With regard to the collision dynamics, the fact of $\lambda \approx R$ tells us that both direct and thermal limits are unrealistic. Keeping these general features in mind, we will look over the data from the next section.

3. PROTON SPECTRA

We first study the proton spectra. In Fig. 5 (upper) the proton spectra measured at c.m. 90° from almost equal-mass collisions, C + C, Ne + NaF, and Ar + KCl, at $E_{\text{beam}}/A = 800$ MeV are plotted.⁴ The spectra are not purely exponential, but resemble each other. This implies that the beam energy per nucleon determines the major dynamics, rather than the total beam energy. We also observe copious production of high energy protons in the region far beyond the free NN kinematical limit (in this case 182 MeV). Even if a proper Fermi motion is included, the production of these high energy protons cannot be explained as a superposition of single NN collisions (the

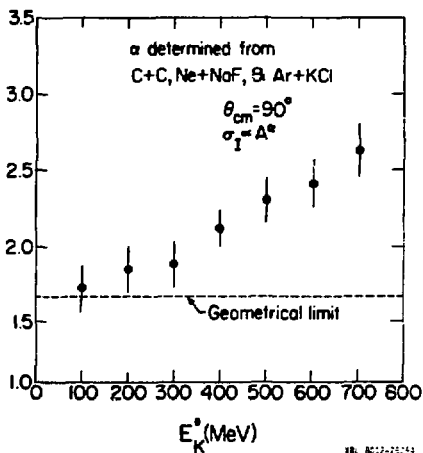
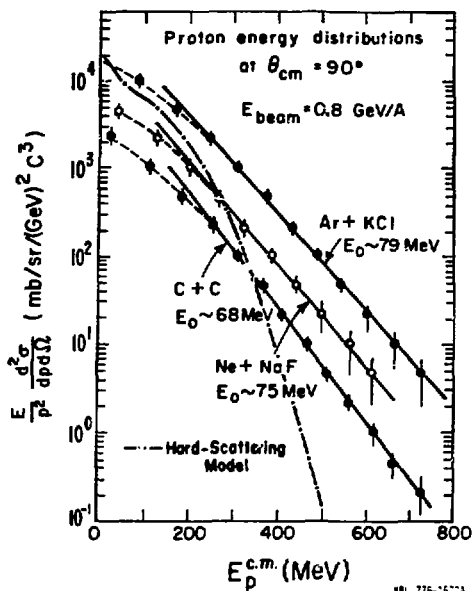


Fig. 5

broken solid curve in Fig. 5 (upper)).

How are these high-energy protons created? In order to study it we parameterize the same data as a power of the projectile (or target) mass number, A , as

$$E(d^2\sigma/d^2p) \propto A^\alpha, \quad (1)$$

and plot this α in Fig. 5 (lower). For low energy protons the value of α is very close to the geometrical limit of $5/3$; in this limit the cross section is proportional to the product of the participating nucleon number ($\propto A$) times the geometrical cross section ($\propto A^{2/3}$).^{4,5} However, in the high energy region $\alpha > 5/3$ and reaches the value of 2.6 or 2.7 at the highest energy. Such a large value of α suggests that multiple NN collision processes are important for the creation of high energy (in this case high p_T) protons.

An extreme limit of the multiple collision is the thermal process. However, in the thermal limit the power α becomes again the geometrical limit of $5/3$.¹⁴ Therefore, the observed power dependence indicates that, although high-energy protons are created from multiple NN collisions, they are not extremely frequent multiple collisions. Then, an immediate question is how many nucleons are actually involved. This question has been studied by many theorists.^{14,15,16} According to a recent calculation,¹⁴ the average number of NN collisions, $\langle n \rangle$, monotonically increases as the observed proton energy increases. The value of $\langle n \rangle \approx 3$ for $E_p^{\text{c.m.}} \approx 200$ MeV and $\approx 4-5$ for $E_p^{\text{c.m.}} \approx 800$ MeV for the Ar + KCl system.

4. COMPOSITE FORMATION

In the presence of multiple collisions, there is a certain chance that these nucleons stick together to form a composite fragment. According to simple phase space considerations, we expect that the probability of forming a deuteron at a velocity \vec{v}_d is proportional to the product of the probabilities of finding a proton and a neutron at the same velocity:

$$P_d(\vec{v} = \vec{v}_d) \propto P_p(\vec{v} = \vec{v}_d) \cdot P_n(\vec{v} = \vec{v}_d). \quad (2)$$

If the neutron spectra can be replaced by the proton spectra,¹⁷ we have

$$E_A(d^2\sigma_A/d^2p_A) = C_A \cdot [E_p(d^2\sigma_p/d^2p_p)]^2 \quad \text{for } p_A = A \cdot p_p. \quad (3)$$

The above power law is called the coalescence model^{18,19} and is tested in Fig. 6 with the data.⁴ With one normalization constant, C_A , this power law holds extremely well.

In order to study this power law in more detail the ratios of observed deuteron cross sections to the squares of observed proton cross sections are displayed in Fig. 7 for Ne + NaF collisions at three bombarding energies, 0.4, 0.8, and 2.1 GeV/nucleon.⁴ The value of C_A is about 15×10^{-6} in units of $[(\text{mb} \cdot \text{GeV})/(\text{sr} \cdot (\text{GeV}/c)^2)]^{-1}$, and it is almost independent of deuteron momentum as well as deuteron emission angle. In addition, the value of C_A is almost independent of the projectile energy.

To what extent does the power law of Eq. (3) hold in terms of theoretical models? Assume that the particle density per unit phase space volume is given by $f(\vec{p})$ such that

$$(1/V) \cdot (d^3n/d^3p) = f(\vec{p}), \quad (4)$$

where V is the phase space volume. Then, the ratio C_A is given by

$$C_A = (1/\gamma V)^{A-1} (f(\vec{p}_A)/[f(\vec{p}_p)]^2) \quad \text{for } p_A = A \cdot p_p. \quad (5)$$

where γ is the Lorentz factor of a particle measured in the frame in which Eq. (4) is defined. First we consider the thermal model in which a macroscopic chemical potential is a driving force to create a composite fragment. In the simplest fireball model,²⁰

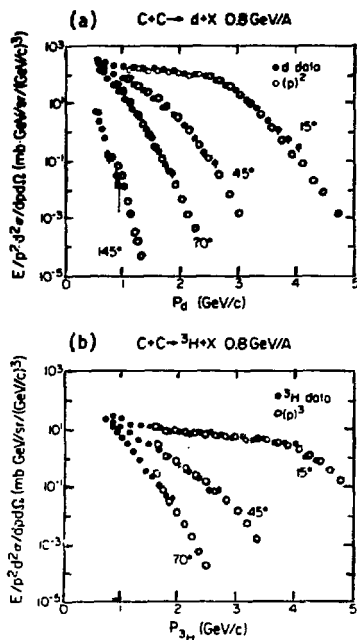


Fig. 6

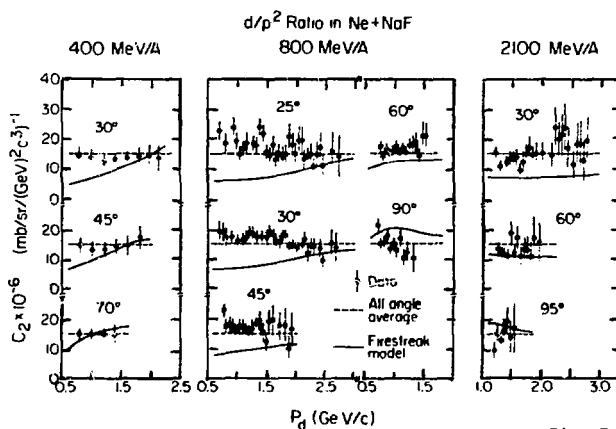


Fig. 7

$$f(p) \propto e^{-E/T}, \quad (6)$$

where E is the kinetic energy of an emitted particle and T is the temperature. Consequently, C_A is given by²¹

$$C_A = \frac{\text{const.}}{(\gamma V)^{A-1}}. \quad (7)$$

The range of γ is 1 - 2 for the data shown in Fig. 7. Therefore, within a factor two this fireball model seems to agree with the observed fact the C_A is almost constant.

However, it has been well known that the simplest fireball model needs to be modified substantially in order to explain the observed large angular anisotropy of various light fragments.⁴ For this purpose the firestreak model^{22,23} was proposed and it has very often been used to fit the experimental data. In this model the nucleus is divided into several tubes in order to reproduce the geometry more realistically than the simplest fireball model. Therefore, the temperature is different from tube to tube, and $f(p)$ is now given by

$$f(p) = \sum_i a_i e^{-E_i/T_i}. \quad (8)$$

In this case C_A is no longer constant and has a strong fragment-energy dependence, as shown in Fig. 7. For example, the predicted value²³ of C_A in the case of 400 MeV/nucleon at 30° (left upper corner in Fig. 7) varies from 5 to 20, depending on the fragment energy, and this clearly disagrees with the data. This fact further implies that composite fragments are unlikely to be produced from a macroscopic chemical equilibrium inside the fireball.

The other model is the coalescence model.^{18,19} According to this model the power law is understood such that, if nucleons are located within a radius of p_0 in the momentum space, then these nucleons stick together to form a composite fragment. In this case C_A is given by^{24,25}

$$C_A = \frac{(N_S/Z_S)^y}{x!y!A^2} \left[\frac{4\pi p_0^3}{3m\sigma_0} \right]^{A-1}, \quad (9)$$

where p_0 is called the coalescence radius. Here, x and y are, respectively, the proton and neutron numbers in the composite particle ($A = x + y$), Z_S and N_S are, respectively, the proton and neutron numbers of the projectile plus target system ($Z_S = Z_P + Z_T$ and $N_S = N_P + N_T$), m is the nucleon mass, and σ_0 is the nucleus-nucleus total cross section.

In this model, if two or more nucleons are located inside the radius p_0 , then the assembly of these nucleons is immediately regarded as a real composite particle. Therefore, the cross section of composite fragment A is expected to be proportional to the A^{th} power of the cross section of original nucleons before the formation of this composite fragment:

$$\sigma_A = C_A [\sigma(\text{original nucleon})]^A. \quad (10)$$

However, the experimental fact is that the power law holds very well between the observed cross sections. Of course, if the cross section for protons is much larger than that for composite fragments, there is no significant difference between Eqs. (10) and (2). But, in certain kinematic regions the ratio of protons to composite fragments is close to one. Still, the power law holds well between the observed cross sections. Therefore, if we use the coalescence model, we must assume local chemical equilibrium between the formation and break-up, such as $d \leftrightarrow p + n$.

In the presence of multiple NN collisions one of important questions is if the macroscopic chemical equilibrium holds. Composite spectra partly answered to this question, namely, it does not seem to hold, although a microscopic chemical

equilibrium between the formation and break-up must exist.

5. PION PRODUCTION

For beam energies of ≈ 1 GeV/nucleon the dominant secondary particles created in collisions are pions. At these energies the pion production proceeds mainly from Δ_{33} excitation of nucleons. Therefore, pion spectroscopy has played a major role in the research of high energy nuclear collisions at $E_{\text{beam}}/A \approx 1$ GeV. Out of a large amount of available data we will select here three subjects: (1) multiplicity, (2) two-pion interferometry, and (3) energy distribution.

The first example is the multiplicity. In Fig. 8 observed multiplicities⁴ for pions and nuclear fragments are plotted as a function of the participant nucleon number, P (or participant proton number, P_Z). The data of nuclear fragments (lower figure) contain mostly the contribution from the participant region, since the data at large angles are used to obtain the multiplicities. We observe $\langle m_p \rangle \propto A^{2/3}$ while $\langle m_Z \rangle \propto P_Z$. This $A^{2/3}$ dependence for pions suggests that pions are strongly absorbed before they are emitted. In other words, pions are emitted after several rescatterings with surrounding nucleons, and thereby display features of the equilibrated stage of the system.

The second is the two-pion interferometry. Suppose that two identical particles such as two negative pions, are created at $(\vec{r}, t) = (\vec{x}_1, t_1)$ and (\vec{x}_2, t_2) , and that these two particles are detected at (\vec{X}_1, T_1) and (\vec{X}_2, T_2) . Then, within the plane-wave approximation, the observed two-particle spectrum is expressed as²⁶⁻³²

$$P(\vec{X}_1, T_1, \vec{X}_2, T_2) = \frac{1}{2} |\exp[i\vec{k}_1(\vec{X}_1 - \vec{x}_1) - iE_1(T_1 - t_1)] \cdot \exp[i\vec{k}_2(\vec{X}_2 - \vec{x}_2) - iE_2(T_2 - t_2)] \\ \pm \exp[i\vec{k}_1(\vec{X}_1 - \vec{x}_2) - iE_1(T_1 - t_2)] \cdot \exp[i\vec{k}_2(\vec{X}_2 - \vec{x}_1) - iE_2(T_2 - t_1)]|^2, \quad (11)$$

where (\vec{k}_i, E_i) are the momentum and energy of a particle detected at (\vec{X}_i, T_i) . The sign of \pm corresponds to bosons (+) and fermions (-), respectively. Since pion is a boson, we discuss the negative sign only. The above equation can be rewritten as

$$P(\vec{X}_1, T_1, \vec{X}_2, T_2) = 1 - \cos[\vec{q}(\Delta\vec{x}) - E_0(\Delta t)], \quad (12)$$

with

$$\vec{q} = \vec{k}_1 - \vec{k}_2, \quad \Delta\vec{x} = \vec{x}_1 - \vec{x}_2, \quad E_0 = E_1 - E_2, \quad \text{and} \quad \Delta t = t_1 - t_2. \quad (13)$$

If the emitting source of pions has a space-time structure given by $\rho(\vec{r}, t)$, then the actual two-pion spectrum, C_2 , is given by

$$C_2 = \int P(\vec{X}_1, T_1, \vec{X}_2, T_2) \rho(\vec{x}_1, t_1) \rho(\vec{x}_2, t_2) d\vec{x}_1 d\vec{x}_2 dt_1 dt_2. \quad (14)$$

For example, in the case where

$$\rho(\vec{r}, t) \propto e^{-r^2/R^2} \cdot e^{-t^2/\tau^2}, \quad (15)$$

we have³¹

$$C_2 = 1 + \exp[-|\vec{q}|^2 R^2 / 2 - E_0^2 \tau^2 / 2]. \quad (16)$$

Therefore, $C_2 = 1$ at $(|\vec{q}|, E_0) \rightarrow \infty$, and $= 2$ at $|\vec{q}| \rightarrow 0$ (in this case E_0 is automatically 0). The width of the shape of C_2 is characterized by R and τ . Namely, from the measurements of the above interference pattern, C_2 , we can determine the source size (R) and the collision time (τ).

Eq. (11) assumes that two pions are emitted from two independent points without any coherence. If these two points are strongly correlated, such as seen in a pion laser, then such an interference pattern disappears.³² The peak height of the

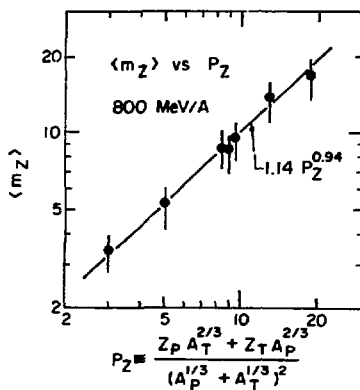
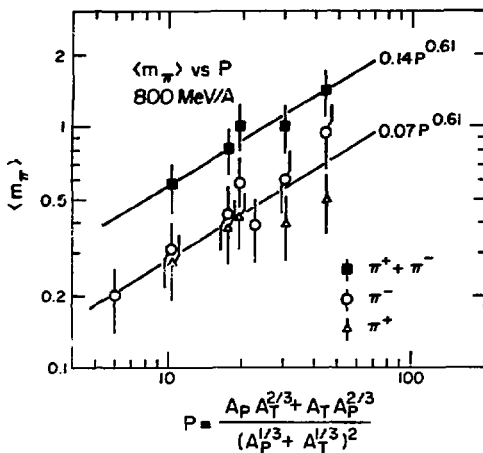


Fig. 8

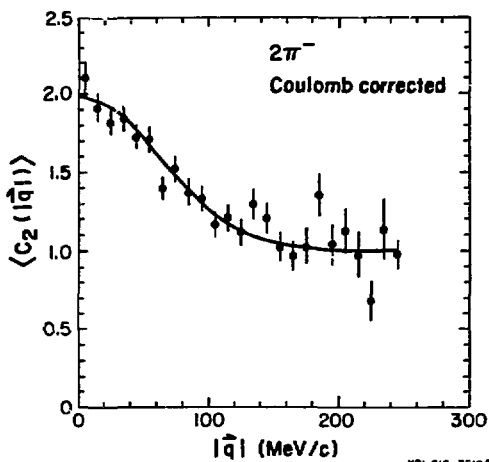
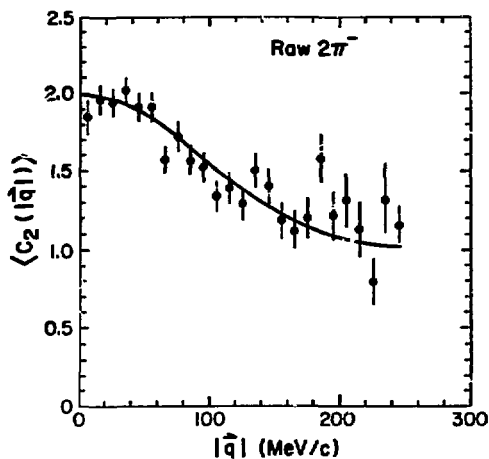


Fig. 9

interference pattern. C_2 may thus tell us the degree of coherence in the pion production.

Recently Zajc *et al.*⁷ have measured rather carefully the two-pion spectra in 1.8 GeV/nucleon Ar + KCl collisions, as shown in Fig. 9. First we note that actual two-pion spectra are largely affected by the final state interactions. These interactions originate both from Coulomb and strong interactions, and especially from the former because $\pi^-\pi^-$ ($T = 2$) strong interactions at small relative momentum are negligibly small. If we apply a standard Gamov correction for Coulomb interactions, then two-pion spectra are significantly changed, as shown in Fig. 9. Therefore, the widths for the raw data do not immediately reflect R and τ . After the Coulomb corrections the value of $R = 3.0 \pm 0.3$ was obtained for the Ar + KCl system. Whether $C_2 = 2$ at $|\vec{q}| \approx 0$ depends on the normalization of the data. They have examined various cases which might affect the normalization of the data. At the present moment, however, no strong evidence on the deviation of C_2 from 2 is observed.

The third example is the energy spectra. As shown in Fig. 10, the spectra at c.m. 90° are almost exponential,

$$E(d^3\sigma/d^3p) \propto \exp(-E_\pi^{\text{c.m.}}/E_0). \quad (17)$$

at any bombarding energy.³⁴ This exponential behavior is a feature generally observed for pions with any projectile and target (with $A > 4$) and at any c.m. angle.

In Fig. 11 the observed values of the slope factor E_0 are plotted as a function of the beam energy per nucleon in the c.m. frame.⁴ E_0 increases monotonically as the beam energy increases. In addition, we notice that the value of E_0 for pions is consistently smaller than that for high-energy protons (see Fig. 5 for the definition of E_0 for high-energy protons).

Several ideas have been proposed to explain the observation of $E_0(\pi) < E_0(p)$, in terms of (1) mean free paths, (2) radially exploding flow³⁴, (3) phase space^{35,36}, and (4) statistics. Inside nuclear matter, the mean free path of protons (≈ 2 fm) is longer than that of pions (≈ 0.5 fm). Therefore, pions may sample a much colder stage of the collisions than protons [possibility (1)]. The second possibility was pointed out by Siemens and Rasmussen.³⁴ At a fixed kinetic energy the velocity of a proton is much smaller than that of a pion. Therefore, if there is an explosive flow, there will be a greater enhancement in kinetic energy for protons than for pions. Consequently, the proton spectra become broader than the pion spectra. This idea explained reasonably well the difference in E_0 as well as the spectrum shapes of both pions and protons, as shown in Fig. 12.³⁷ The third possibility is related to the NN kinematics. In order to create pions the 140 MeV rest-mass energy has to be supplied. Then, the average kinetic energy available for pions is less than that for protons. The fourth possibility is less important than the previous three, but may induce an additional effect. In the very low energy region the boson (pion) yield could increase more than exponential whereas the fermion (proton) yield could be suppressed, because of statistics. From the comparison between the proton and pion spectra alone, it is hard to prove which of these four mechanisms is most important. With the aid of K^+ spectra, a certain answer is obtained, as we will discuss in the next section.

Before finishing this section I will add one comment on the production of high-energy pions with 183 MeV/nucleon Ne + NaF collisions, as shown in Fig. 10. In nuclear collisions at laboratory beam energies below 290 MeV/nucleon (which is the pion production threshold energy in free NN collisions), pion production is due either to the nucleon Fermi motion or due to an accumulation of available energy greater than $m_{\pi c^2}$ through successive NN collisions. In Fig. 10 the highest kinetic energy of pions observed in this experiment is 260 MeV in the NN c.m. frame. In order to create such pions, a total energy (including the 140 MeV rest mass) of 400 MeV has to be supplied. If there were no internal momenta of the nucleons in both the projectile and target

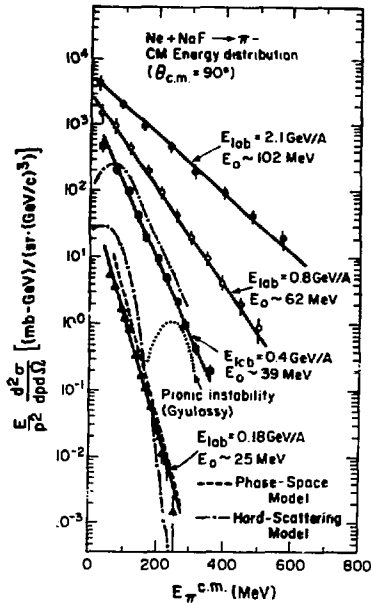
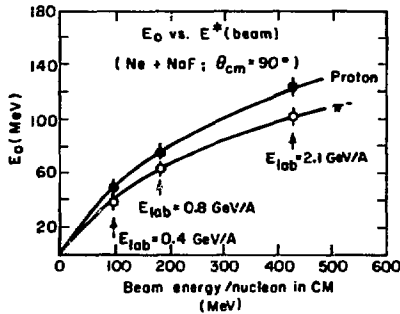


Fig. 10

XBL 8112-13255



XBL 788-1495B

Fig. 11

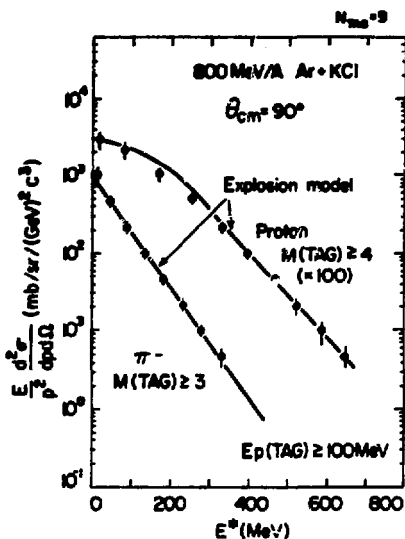


Fig. 12

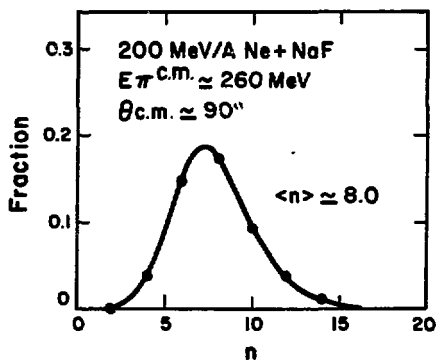


Fig. 13

nuclei, each nucleon would carry 45 MeV kinetic energy in the c.m. frame. In this case, at least nine nucleons would have to sum their kinetic energies to create such a pion. On the other hand, if these pions are created in the single NN collisions, then an extremely large Fermi momentum (up to 600 MeV/c) has to be assumed. In either case the production mechanism is of substantial theoretical interests.

Two theoretical models are compared with the data. One is the phase-space model,^{30,38} since this model explains quite well the existing pion data at higher beam energies. The cross section calculated with this model is shown by the dashed line in Fig. 10. The agreement with the data is reasonably good. In this model the calculated distribution of nucleon number, n , for the creation of 280 MeV pion in the c.m. frame is shown in Fig. 13. The average number, $\langle n \rangle \approx 6$, is almost the same as what we guessed on the basis of simple energy considerations as described above. Hard-collision-model calculations,³⁹ on the other hand, do not fit the data well. Of course, there are still many problems in both theoretical models, but we can tentatively conclude that the process involving more than two nucleons has to be considered carefully and correctly in order to explain the production of high-energy pions at subthreshold beam energies.

8. PRODUCTION OF STRANGE PARTICLES

In Fig. 14 various threshold energies for particle production in NN collisions are displayed. As the beam energy increases (above 2 GeV) the production of strange particles becomes important.

Schnetzer *et al.*³⁰ have measured K^+ spectra with a magnetic spectrometer. The motivation of this experiment is as follows: Since the cross section of $K^+ + N$ (≈ 10 mb) is much smaller than that of $N + N$ (≈ 40 mb) or $\pi + N$ (≈ 100 mb), once K^+ is created, it is less likely to be rescattered by surrounding nucleons. In other words, K^+ may be a more reliable messenger than π or proton of the violent initial, and perhaps, very compressed and hotter stage of the nuclear collision. In Fig. 15 an example of energy spectra in the c.m. frame is plotted for 2.1 GeV per nucleon Ne + NaF collisions. The spectrum shape is almost exponential with inverse exponential slope, $E_0 \approx 142$ MeV. This value of E_0 is larger than E_0 for protons or pions (see Fig. 11), implying that K^+ 's seem to be created at a much more violent stage than pions or protons. The exponential behavior of the spectrum is a general feature for any projectile (even p or d) on nuclear targets. In addition, the angular distribution of K^+ is almost isotropic in the NN c.m. frame.

Comparison of the value E_0 for K^+ with that for pion and proton may give us further insight into the production mechanism of these particles (see the previous section). If the mean free path of the product particle mainly determine the slope E_0 , then we expect

$$E_0(\pi) < E_0(p) < E_0(K^+), \quad (18)$$

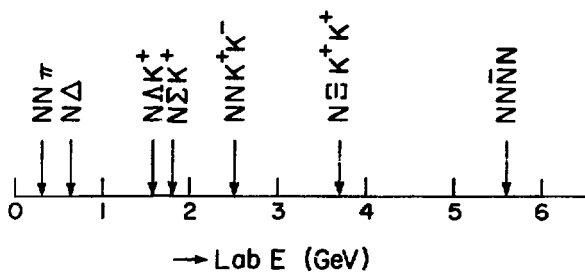
since $\lambda(\pi) < \lambda(p) < \lambda(K^+)$. This relation agrees with the experiment. On the other hand, if the phase space of particle production determines the shape of the energy spectrum we expect

$$E_0(K^+) < E_0(\pi) < E_0(p), \quad (19)$$

since the threshold energy of K^+ production is much higher than that of π production, so that less kinetic energies are available for K^+ . Since this relation is not satisfied in the experimental data, the observed energy spectrum seems to justify the explanation that K^+ reflects the most violent stage of the collision because of its long mean free path.

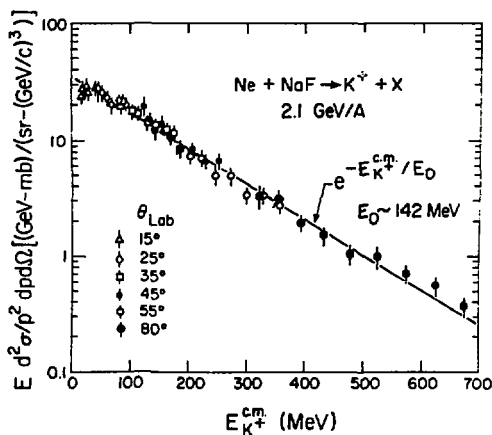
Then, how do we explain the data? So far, no satisfactory explanation has been available. Recently a linear cascade calculation based on row-on-row straight-line

Particle Production Threshold in NN Collision



XBL816-2358

Fig. 14



XBL 816-236

Fig. 15

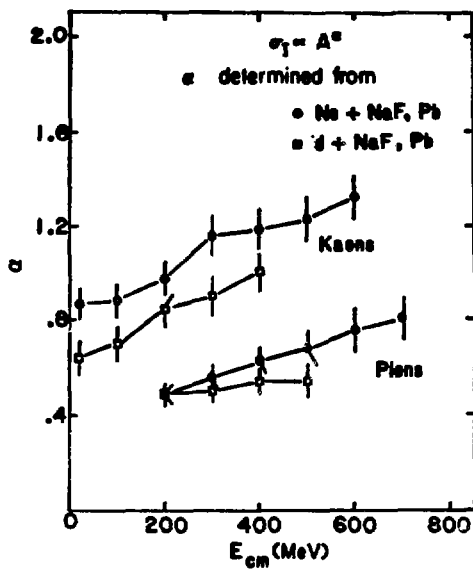


Fig. 16

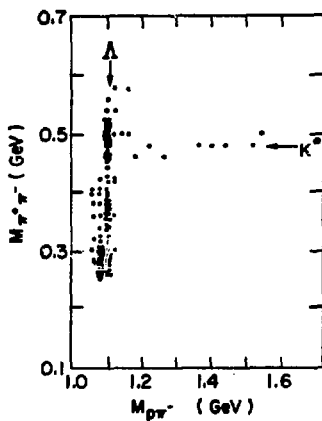


Fig. 17

geometry succeeded in reproducing the shape of the energy spectrum, by including a slight rescattering of K^+ by surrounding nucleons.³⁹ However, this calculation fails to reproduce the angular distribution, especially for the case of proton + nucleus collisions. Therefore, this point remains an open question.

An interesting aspect of K^+ data is seen in the A dependence. If the cross section is parameterized as a power of A_T ($\propto A_T^\alpha$), then the value of α is consistently larger for Ne projectiles than for d projectiles, as seen in Fig. 16. From a simple geometrical consideration we expect the opposite trend, since with a heavier-mass projectile the increase of target size must have less effect on the yield (in fact, we expect $\propto A_T^{2/3}$ for heavy-mass projectiles and $\propto A_T$ for light-mass projectiles). Perhaps this experiment indicates that, with heavier-mass projectiles the compressed and hot region is created more copiously than with lighter-mass projectiles. Such a feature is not (or is only slightly) observed for pion production, as seen in Fig. 18.

The Λ production has been studied recently by Harris *et al.*⁴⁰ with a streamer chamber in 1.8 GeV per nucleon Ar + KCl collisions. In this measurement the decay of Λ ,

$$\Lambda \rightarrow p + \pi^- \quad (64\% \text{ branching}), \quad (20)$$

was used for the identification of Λ , as shown in Fig. 17. Clearly, Λ is observed.

Although statistics of the data are low, a large number of Λ 's which have momenta larger than expected from free NN collisions are observed. This is consistent with the previous data of K^+ .

It is well known that the decay of Λ shown in Eq. (20) is through weak interactions. Therefore, if Λ has a polarization, P , the angular distribution of the decay products have angular anisotropy expressed as

$$W(\vartheta) = 1 + \alpha P \cos \vartheta, \quad (21)$$

where ϑ is the emission angle of p with respect to the polarization axis and $\alpha = -0.64$ in this case. By defining the reaction plane such that the beam and the emitted Λ form this plane, the value of P has been determined to $P = -0.10 \pm 0.05$. In terms of the quark model, Λ is described as (uds) in which spins of u and d are coupled to zero. Therefore, the polarization of Λ readily measures the polarization of s -quark. Measurements of Λ polarization are thus interesting and perhaps useful for studying the role of quarks in high energy nuclear collisions.

K^- has recently been measured with a magnetic spectrometer.⁴¹ In this case, the yield is extremely low, since the Bevalac maximum energy is 2.1 GeV per nucleon while the threshold energy of K^- in NN collision is 2.6 GeV. Therefore, the data only tell us the integrated yield of K^- . Although these data were compared with various model calculations, I would say that meaningful physics can be extracted only when we have more data at higher statistics.

7. SUMMARY

In this talk I have given a quick overview of light particle spectra from which we have studied the reaction mechanisms involved in the emission of these particles. Obviously more data exist. Among them the particle correlation data are especially important for the study of the reaction mechanism. Although I was not able to cover this subject in this talk, if some of you are interested in it, see for example, Refs. 42 and 43.

Let me summarize what we have learned so far.

- (1) Individual NN collisions seem to determine the basic dynamics of the nucleus-nucleus collisions at $E_{\text{beam}}/A \approx 1$ GeV/nucleon.
- (2) The participant-spectator model is a reasonable description of the geometrical

aspect of the collision.

- (3) Beam energy per nucleon (rather than the total beam energy) determine the major dynamics.
- (4) High- p_T protons are mainly from multiple NN collisions but not extremely frequent multiple collisions.
- (5) A power law holds extremely well between the *observed* composite-fragment spectra and the *observed* proton spectra. This fact further implies that the macroscopic chemical equilibrium does not hold, whereas the microscopic chemical equilibrium seems to hold.
- (6) The observed mass dependence of pion multiplicity suggests the importance of the pion absorption process.
- (7) Effects of final-state interactions sensitively reflect two-pion spectra at small relative momenta. After the correction of these interactions, the source radius has been determined to be about 3 fm for the Ar + KCl system.
- (8) No coherence effect of pion emission is observed.
- (9) Spectra for π 's and K^* 's are approximately exponential, while those for protons are not purely exponential. Exponential slopes satisfy the relation of $E_0(\pi) < E_0(p) < E_0(K^*)$, implying that K^* is sensitive to the most violent stage, while π is sensitive to the equilibrated "cold" stage of the collision.
- (10) High-energy pion emission at subthreshold beam energies requires a process involving more than two nucleons.
- (11) There is a puzzle in the target-mass dependence of the K^* cross section, namely, if the cross section is parameterized to A^α , the value of α for Ne projectiles is consistently larger than that for d projectiles. It may suggest that the initial "hot" region may be created more easily with heavier-mass combinations between the projectile and target.
- (12) Polarization of Λ is observed at $E_{\text{beam}}/A = 1.8$ GeV to $P = -0.10 \pm 0.05$, although no polarization has been observed in pp collisions at 2 GeV energy region.

Keeping this basic knowledge in mind I will discuss on Thursday the current puzzles and future possibilities.

ACKNOWLEDGMENTS

The work was supported by the Director, Office of Energy Research, Division of Nuclear Physics of the Office of High Energy and Nuclear Physics of the U.S. Department of Energy under Contract W-7405-ENG-48. It was also supported by the INS-LBL Collaboration Program.

REFERENCES

- † From March 1st, also Department of Physics, Faculty of Science, University of Tokyo, Hongo, Bunkyo-ku, Tokyo, Japan.
1. J. D. Bowman, W. J. Swiatecki, and C. F. Tsang, Lawrence Berkeley Laboratory Report LBL-2906 (1973), unpublished.
2. L. Anderson, W. Brückner, E. Moeller, S. Nagamiya, S. Nissen-Meyer, L. Schroeder, G. Shapiro, and H. Steiner, preprint (1982).
3. J. V. Geaga, S. A. Chessin, J. Y. Grossiord, J. W. Harris, D. L. Hendrie, L. S. Schroeder, R. N. Treuhaft, and K. Van Bibber, Phys. Rev. Lett. 45, 1993 (1981).
4. S. Nagamiya, M.-C. Lemaire, E. Moeller, S. Schnetzer, G. Shapiro, H. Steiner, and I. Tanihata, Phys. Rev. C24, 971 (1981).
5. S. Nagamiya, Nucl. Phys. A335, 517 (1980).
6. I. Tanihata, S. Nagamiya, S. Schnetzer, and H. Steiner, Phys. Lett. 100B, 121 (1981).
7. W. A. Zajc, J. A. Bistirlich, R. R. Bossingham, H. R. Bowman, C. W. Clawson, K. M.

- Crowe, K. A. Frankel, O. Hashimoto, J. G. Ingersoll, M. Koike, J. P. Kurck, C. J. Martoff, W. J. McDonald, J. P. Miller, D. Murphy, J. O. Rasmussen, J. P. Sullivan, P. Truol, and E. Yoo, in Proc. 5th High Energy Heavy Ion Summer Study, LBL-12852, Conf-8105104, Berkeley, May, 1981, p.350.
8. S. Y. Fung, W. Gorn, G. P. Kiernan, J. J. Lu, Y. T. Oh, and R. T. Poe, Phys. Rev. Lett. 41, 1592 (1978).
 9. J. J. Lu, D. Beavis, S. Y. Fung, W. Gorn, A. Huie, G. P. Kiernan, R. T. Poe, and G. VanDalen, Phys. Rev. Lett. 46, 898 (1981).
 10. Z. Zerbakhsh, A. L. Sagle, F. Brochard, T. A. Mulera, V. Perez-Mendez, I. Tanihata, J. B. Carroll, K. S. Ganezer, G. Igo, J. Oostens, D. Woodard, and R. Sutter, Phys. Rev. Lett. 46, 1288 (1981).
 11. For example, I. A. Schmidt and R. Blankenbecler, Phys. Rev. D15, 3321 (1977); Phys. Rev. D18, 1318 (1977).
 12. A review of the thermal model is given by S. Das Gupta and A. Z. Mekjian, Phys. Reports 72, 131 (1981).
 13. Reviews of the hydrodynamical model are given by J. R. Nix, Prog. Part. Nucl. Phys. 2, 237 (1979); H. Stöcker, J. Hofmann, J. A. Maruhn, and W. Greiner, Prog. Part. Nucl. Phys. 4, 133 (1980).
 14. B. Schürmann and N. Macoc-Borstnik, preprint (1981).
 15. J. Randrup, Phys. Lett. 76B, 547 (1978).
 16. J. Knoll, Phys. Rev. C20, 773 (1979).
 17. W. Schimmerling, J. Kast, D. Orstedahl, R. Madey, R. A. Cecil, B. D. Anderson, and A. R. Baldwin, Phys. Rev. Lett. 43, 1985 (1979).
 18. S. F. Butler and C. A. Pearson, Phys. Rev. 129, 836 (1963).
 19. A. Schwarzschild and C. Zupancic, Phys. Rev. 229, 854 (1983).
 20. G. D. Westfall, J. Gosset, P. J. Johansen, A. M. Poskanzer, W. G. Meyer, H. H. Gutbrod, A. Sandoval, and R. Stock, Phys. Rev. Lett. 37, 1202 (1976).
 21. J. I. Kapusta, Phys. Rev. C21, 1301 (1980).
 22. W. D. Myers, Nucl. Phys. A296, 177 (1978).
 23. J. Gosset, J. I. Kapusta, and G. D. Westfall, Phys. Rev. C18, 844 (1978).
 24. H. H. Gutbrod, A. Sandoval, P. J. Johansen, A. M. Poskanzer, J. Gosset, W. G. Meyer, G. D. Westfall, and R. Stock, Phys. Rev. Lett. 37, 867 (1976).
 25. M.-C. Lemaire, S. Nagamiya, S. Schnetzer, H. Steiner, and I. Tanihata, Phys. Lett. 85B, 38 (1979).
 26. R. Hanbury-Brown and R. Q. Twiss, Nature 178, 1046 (1956).
 27. G. Goldhaber, S. Goldhaber, W. Lee, and A. Pais, Phys. Rev. 120, 300 (1960).
 28. G. I. Kopylov, Phys. Lett. 50B, 572 (1974).
 29. G. Cocconi, Phys. Lett. 49B, 459 (1974).
 30. S. E. Koonin, Phys. Lett. 70B, 43 (1977).
 31. F. B. Yano and S. E. Koonin, Phys. Lett. 78B, 556 (1978).
 32. M. Gyulassy and S. K. Kauffmann, and L. W. Wilson, Phys. Rev. C20, 2267 (1979).
 33. S. Nagamiya, H. Hamagaki, P. Hecking, R. Lombard, Y. Miake, E. Moeller, S. Schnetzer, H. Steiner, S. Kadota, I. Tanihata, S. Bohrmann, and J. Knoll, Lawrence Berkeley Laboratory Report LBL-14033 (1982).
 34. P. J. Siemens and J. O. Rasmussen, Phys. Rev. Lett. 42, 844 (1979).
 35. J. Knoll, Phys. Rev. C20, 773 (1979).
 36. S. Bohrmann and J. Knoll, Nucl. Phys. A356, 498 (1981).
 37. S. Nagamiya, M.-C. Lemaire, S. Schnetzer, H. Steiner, and I. Tanihata, Phys. Rev. Lett. 45, 602 (1980).
 38. S. Schnetzer, Thesis, Lawrence Berkeley Laboratory Report LBL-13727 (1981), unpublished; S. Schnetzer, M.-C. Lemaire, R. Lombard, E. Moeller, S. Nagamiya, G. Shapiro, H. Steiner, and I. Tanihata, to be published.
 39. J. Randrup, Phys. Lett. 99B, 9 (1981).
 40. J. W. Harris, A. Sandoval, R. Stock, H. Stroebele, R. E. Renfordt, J. V. Geaga, H. G. Pugh, L. S. Schroeder, K. L. Wolf, and A. Dacal, Phys. Rev. Lett. 47, 229 (1981).

41. A. Shor, K. Ganzer, J. Carroll, G. Igo, J. Geaga, S. Abachi, A. Sagle, T. Mulera, V. Perez-Mendez, P. Lindstrom, F. Zabakhsh, and D. Woodard, in Proc. 5th High Energy Heavy Ion Summer Study, LBL-12852, Conf-8105104, Berkeley, May, 1981, p.470.
42. S. Nagamiya and M. Gyulassy, to be published in *Advances in Nuclear Physics* [Preprint, Lawrence Berkeley Laboratory Report LBL-14035 (1982)].
43. S. Nagamiya, to be published in *Sov. J. Particles and Nuclei* [Preprint, Lawrence Berkeley Laboratory Report LBL-14034 (1982)].